3 Surface/Interface Magnetism Project

– Crystalline, magnetic and electronic structures at the surface and interface of magnetic thin films and multilayers –

Project Leader: Kenta Amemiya

3-1 Introduction

The surface and interface of magnetic thin films play essential roles in the appearance of extraordinary magnetic properties such as perpendicular magnetic anisotropy (PMA) and the giant magnetoresistance effect. We have investigated the crystalline, magnetic and electronic structures at the surface and interface of magnetic thin films and multilayers, in order to reveal the origin of fascinating magnetic properties that cannot be realized in bulk materials. In this project, various experimental techniques are complementarily used, e.g., depth-resolved X-ray magnetic circular dichroism (XMCD) [1, 2], extended X-ray absorption fine structure (EXAFS), and polarized neutron reflectivity (PNR) [3]. We also planned to perform a muon spin rotation experiment using an ultra-slow muon source, but were unable to do so mainly due to the earthquake in 2011 and some troubles in J-PARC. We have studied magnetic anisotropy of Fe/Ni multilayers [4-7], magnetic structures at the interface between antiferromagnetic FeMn and ferromagnetic Ni [8, 9], effects of ion irradiation on the magnetism of ultrathin films [10, 11], and electric field-induced changes in the magnetic behavior of Fe and FeCo thin films grown on a ferroelectric $BaTiO_3$ substrate [12, 13] and of NiO/Ni thin films grown on a Cu substrate.

3-2 Development of experimental techniques

We have developed some experimental techniques in the last six years. In the soft X-ray region, the 10 Hz polarization switching technique has been developed since 2010 to realize high-sensitivity XMCD measurement, in cooperation with the accelerator laboratory in KEK [14, 15]. A

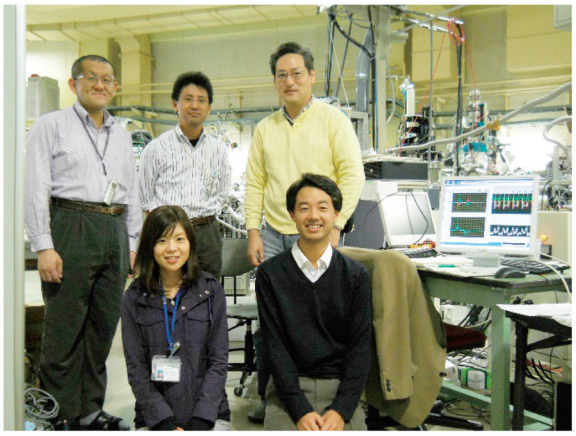

Fig. 1: First XMCD measurement with 10 Hz polarization switching at BL-16A in the Photon Factory.

weak XMCD signal as small as 0.1% can be detected by using the switching between right- and left-hand circular polarizations. This technique is quite effective to measure element- and chemical state-specific magnetization curves by using XMCD, because time-dependent slow changes in the background level of the XMCD data are eliminated owing to the fast switching. Moreover, we have recently succeeded in depth-resolved XMCD measurement with polarization switching, by using a multi-anode microchannel-plate detector, as a project in the open source consortium of instrumentation (Open-it) [16].

Another important experimental progress is the realization of XMCD, EXAFS, and PNR measurements under electric fields. We have developed sample holders, by which voltages of up to 1 kV can be applied between the surface of the thin film and the bottom of the substrate. For example, the sample holder for the PNR measurement is shown in Fig. 2. In addition, a soft X-ray fluorescence detector (microchannel plate) has been introduced to obtain XMCD signals in the soft X-ray

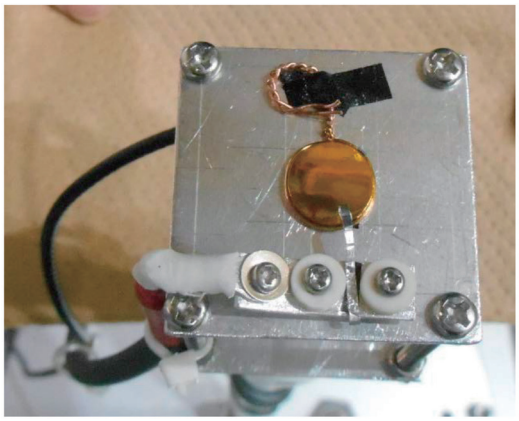

Fig. 2: Sample holder for the PNR measurement under electric fields. A voltage of up to ±1 kV is applied to the film surface via an Al electrode, while the bottom of the substrate is grounded.

region, because electron-yield measurement is difficult under an electric field.

We have also developed some experimental apparatus, such as the 1.2 T-XMCD system with a yoke electromagnet, 5 T-XMCD system with a superconducting electromagnet, and fluorescence-yield depth-resolved XMCD system. By combining these new apparatuses with those developed before this project, we have carried out pioneering science in surface and interface magnetism.

3-3 Scientific topics

This report describes two scientific topics which have been studied by complementary use of X-rays and neutrons. XMCD and EXAFS measurements in the soft and hard X-ray regions were carried out mainly at BL-16A and BL-12C, respectively, in the Photon Factory, while the PNR data were recorded at BL-17 (SHARAKU) in MLF, J-PARC.

3-3-1 Twisted magnetic moment at the interface between ferromagnetic Ni and antiferromagnetic FeMn [8, 9]

The magnetic anisotropy interaction between antiferromagnetic (AFM) and ferromagnetic (FM) materials has been extensively investigated [17, 18]. It was reported that the magnetic easy axis of ~10 monolayer (ML) Ni films switches from the perpendicular to in-plane directions when the films are attached to an AFM FeMn film [17], which indicates that the AFM FeMn film enhances in-plane magnetic anisotropy. The change in magnetic anisotropy induced by AFM FeMn is

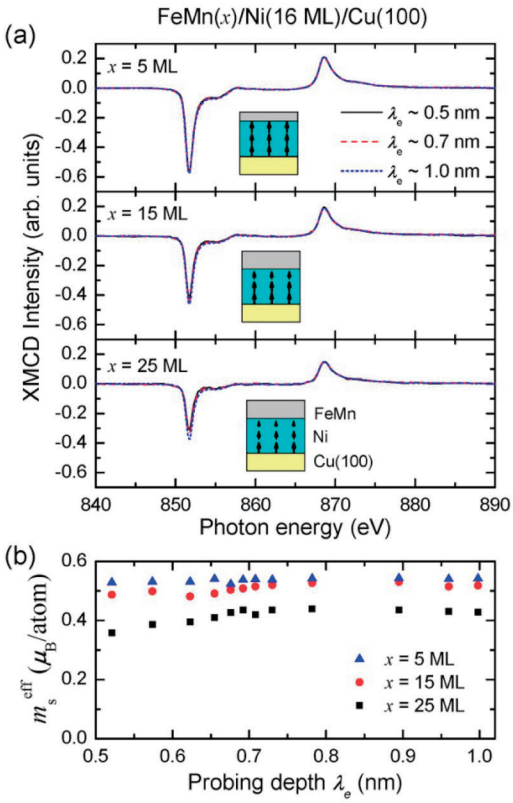

Fig. 3: Probing depth (λ_e) dependence of (a) normal-incidence Ni L-edge XMCD spectrum for FeMn(x)/Ni(16 ML)/Cu(100) and (b) averaged effective spin magnetic moment m_s^{eff} estimated by applying the sum rules to each spectrum.

explained by the magnetic frustration between Ni and FeMn, i.e., since each atomic layer in FeMn has net perpendicular magnetization which is opposite to that in the adjacent layer, the magnetic moment in perpendicularly magnetized Ni undergoes a frustration at the FeMn/Ni interface if the interface has atomic-layer steps.

To investigate the magnetic structure at the interface between AFM FeMn and FM Ni, the Ni L-edge depth-resolved XMCD spectra were measured for FeMn/Ni/Cu(100) samples with 16 and 7.5 ML Ni [8]. In the case of a film with the Ni thickness of 16 ML, which shows perpendicular magnetization in the remanent state (Fig. 3), the perpendicular magnetic component in Ni decreases as the probing depth decreases, i.e., as the surface sensitivity increases.

On the other hand, in the case of 7.5 ML Ni, which shows in-plane magnetization in the remanent state (Fig. 4), the in-plane magnetic moment does not decrease but is almost constant independent of the probing depth. By comparing the results for 16 and 7.5 ML Ni, it is suggested that the magnetic moment in Ni prefers the in-plane direction around the interface with FeMn. Therefore,

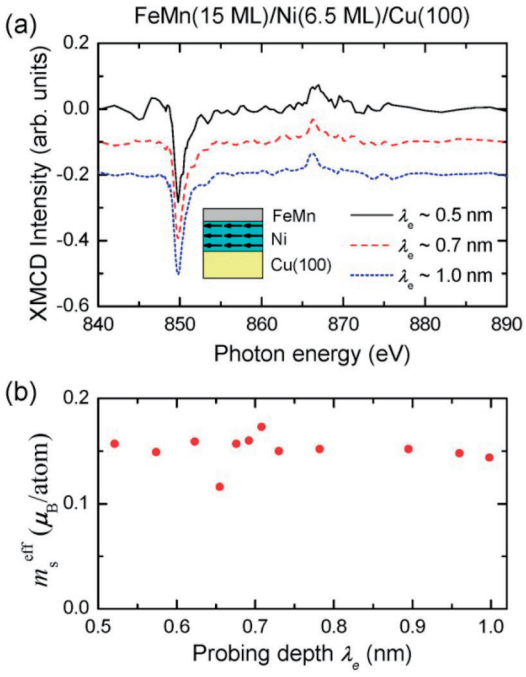

Fig. 4: Probing depth (λ_e) dependence of (a) grazing-incidence Ni L-edge XMCD spectrum for FeMn(15 ML)/Ni(16 ML)/Cu(100) and (b) averaged effective spin magnetic moment m_s^{eff} estimated by applying the sum rules to each spectrum.

a twisted magnetic structure is expected to be realized when a weak in-plane magnetic field is applied to an FeMn/Ni film which shows perpendicular magnetization in the remanent state.

Next, we applied the PNR technique in order to confirm the existence of the twisted magnetic moment around the interface between AFM FeMn and FM Ni, and to reveal the magnetic field dependence of the twisted moment. The PNR experiment was carried out at BL-17 (SHARAKU) using a pulsed neutron source [3]. Magnetic fields, *H*, of up to 10 kOe were applied along the film plane, and the neutron polarization was also in the film plane. The PNR measurement was performed at

Fig. 5: PNR experiments at BL-17 (SHARAKU) in MLF, J-PARC.

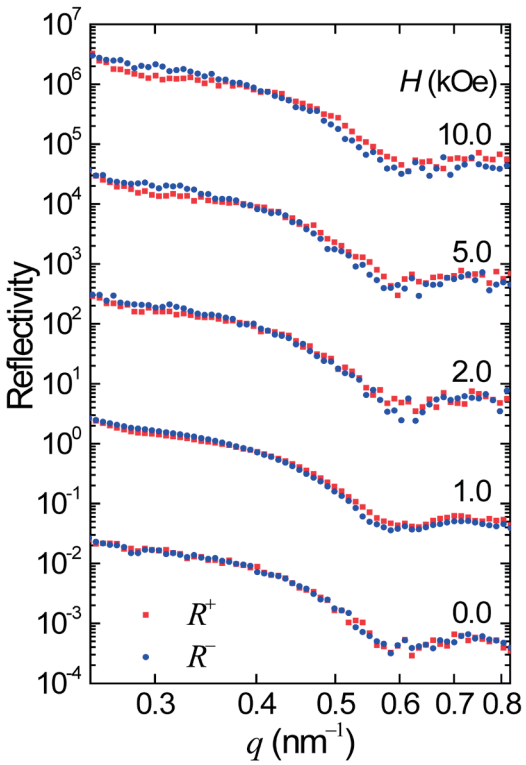

Fig. 6: PNR curves, *R*+ and *R*−, for Cu/FeMn/Ni/Cu(100) measured at different magnetic fields, *H*. The data for different *H* are vertically shifted.

room temperature. A Cu/FeMn/Ni/Cu(100) film, which exhibits perpendicular magnetization in the remanent state, was investigated.

Figure 6 shows PNR curves for Cu/FeMn/Ni/Cu(100) taken at different in-plane magnetic fields, *H*. The Cu, FeMn and Ni layer thicknesses were ~70, ~20, and ~11 ML, respectively. Since the film shows perpendicular magnetization in the remanent state, the PNR data reflects the in-plane component of the magnetic moment induced by the magnetic field. In fact, the difference between R^+ and R^- is undetectable at $H = 0$ kOe, and it gradually increases with increasing *H*. Then the observed PNR curves are fitted by using a two-region model, in which the Ni film is separated into two regions, the interface and inner part of the film, which have different in-plane magnetic moments. Since the net in-plane magnetic moment in each atomic layer of FeMn vanishes due to the AFM coupling, the magnetic structure of FeMn was not considered in the fitting procedure. We optimized the magnetic moments in the interface and inner regions for each *H*, while the other parameters, scattering length density (SLD), film thickness, and roughness, were assumed to be the same for all *H*. To

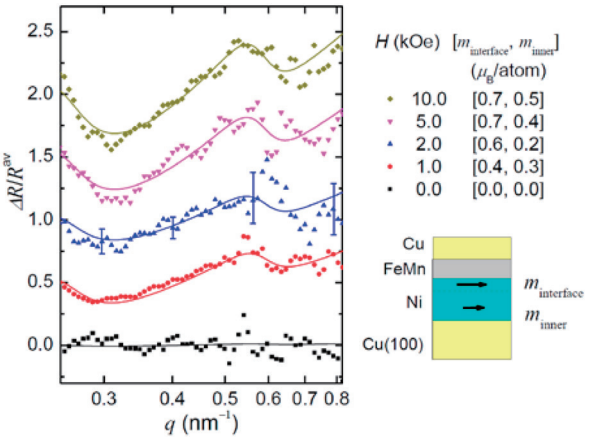

Fig. 7: Difference in the PNR curves, $\Delta R = R^+ - R^-$, divided by the average of them, $R_{av} = (R^+ + R^-)/2$, for Cu/FeMn/Ni/Cu(100) measured at different magnetic fields, H. The data for different H are vertically shifted. The lines are the simulated curves using the in-plane magnetic moments in the interface and inner regions of the Ni film, $m_{interface}$ and m_{inner}, respectively, indicated in the figure.

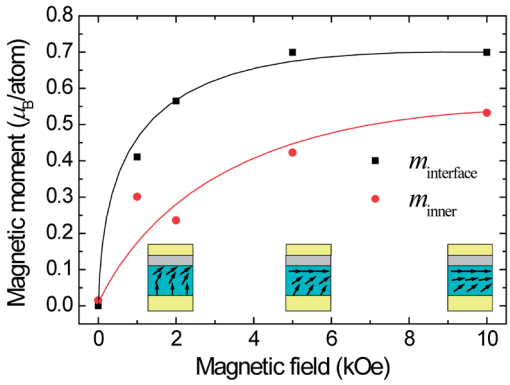

Fig. 8: In-plane component of the magnetic moment in the interface and inner region of the Ni film, estimated by fitting the PNR curves, as a function of applied magnetic field, H. The lines are guides for the eye. The expected magnetic structure is schematically illustrated.

emphasize the magnetic contribution in the PNR curve, $\Delta R/R_{av}$ is plotted in Fig. 7, together with the fitting result. Here, $\Delta R = R^+ - R^-$, and R_{av} represents the average between R^+ and R^-. The overall shape of $\Delta R/R_{av}$ is basically the same for all H, but it is clear that the magnetic field dependence cannot be explained by just multiplying the $\Delta R/R_{av}$ curves by scaling factors.

Figure 8 shows the magnetic field (H) dependence of the in-plane components of the magnetic moment in the interface and inner regions of the Ni film obtained from the PNR analysis. It is revealed that the magnetic moment around the interface with FeMn rapidly rotates to the in-plane direction with increasing H, which leads to the twisted magnetic structure as discussed above. At higher H, the magnetic moment in the inner region also aligns in the in-plane direction as illustrated in Fig. 3. It is thus suggested that the anomalous magnetic behavior is due to the magnetic anisotropy interaction between the AFM FeMn and FM Ni.

3-3-2 Electric field-induced changes in magnetization and structure of Fe thin films grown on $BaTiO_3$

One of the most usual ways to control the direction of the spin moment in a magnetic material is to apply a magnetic field generated by an electromagnet. It requires a relatively large current to generate a magnetic field. On the other hand, it has been shown that the spin direction can be switched by a spin polarized current, in which a much smaller current is required compared with the switching by a magnetic field, especially in the case of nanometer-scale magnets such as those in a magnetic recording device. Moreover, electric field-induced magnetization switching was recently demonstrated [19], which has great potential to reduce the energy consumed in the magnetization switching process.

The idea of controlling magnetization by an electric field has been proposed as the "multiferroic" concept [20]. For instance, $BiFeO_3$ has been extensively investigated as one of the most promising multiferroic materials. Unfortunately, the temperature at which such materials show the multiferroic property is usually far below room temperature in the case of single compound materials. On the other hand, it was reported that the coercive field of a ferromagnetic Fe thin film grown on a ferroelectric $BaTiO_3$ (BTO) substrate changes when a voltage is applied between the Fe film and the bottom of the substrate, even at room temperature [21]. Since the mechanism of the electric field-induced effects on the magnetic properties is not clearly understood, we have performed XMCD, PNR, and EXAFS measurements for Fe thin films grown on the BTO substrate, and observed the changes in the interface state induced by electric polarization of the substrate. Fe L-edge XMCD and Fe K-edge EXAFS spectra were taken at BL-16A and BL-12C of the Photon Factory, while PNR was measured at BL-17 (SHARAKU) in MLF, J-PARC.

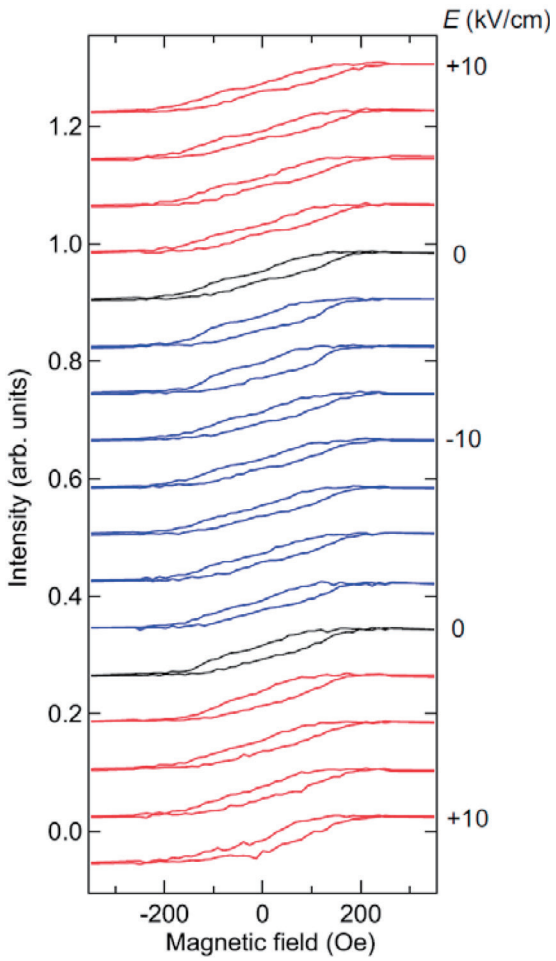

Fig. 9: XMCD-hysteresis curves measured at the Fe L_3 absorption edge of 8-nm Fe thin film on the BTO substrate at different electric fields, *E*.

Figure 9 displays the XMCD-hysteresis curves measured at the Fe L_3 absorption edge (707.5 eV) of an 8-nm Fe thin film grown on the BTO substrate at different electric fields, *E*. All the curves show small squareness ratio, which indicates that the Fe film shows weak in-plane magnetic anisotropy. Under such magnetic conditions, the magnetic domain structure of Fe could be influenced by the ferroelectric domain structure of the BTO substrate.

Figure 10 shows the electric field dependence of the residual magnetization, M_0 (a), and the coercive field, H_c (b). The electric field is changed from E = 10 kV/cm, as indicated by the arrows in the figure. Both M_0 and H_c show the maximum at ~ ±3 kV/cm, and a hysteresis behavior is observed. Indeed, it is known that the ferroelectric domain of BTO under the tetragonal phase shows a multi-domain structure after going through the zero-field during the polarization reversal. We assume that the coercive field of Fe increases because of the multi-domain formation, which obstructs the

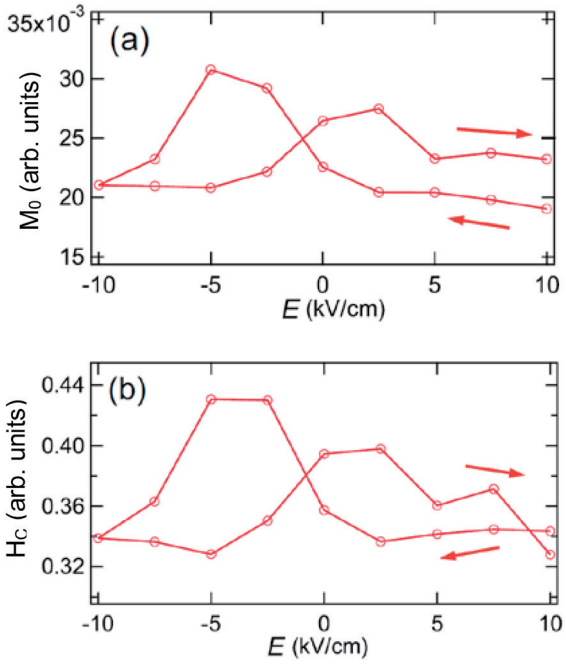

Fig. 10: Electric field dependence of the residual magnetization, M_0 (a), and the coercive field, H_c (b). The electric field is changed from 10 kV/cm, as indicated by the arrows.

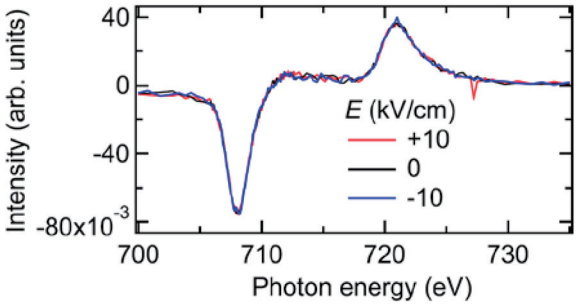

Fig. 11: XMCD spectra of 8-nm Fe film on the BTO substrate measured at the electric field of +10, 0 and −10 kV/cm.

movement of the magnetic domains.

Figure 11 displays the XMCD spectra of the 8-nm Fe film on the BTO substrate. No significant difference by the electric polarization reversal is observed in the spectra. This result indicates that the change in M_0 and H_c by the electric polarization reversal is not caused by the change in the electronic state of Fe itself, but by the ferroelectric domain structure of the BTO substrate. Because the domain structure of BTO is expected to affect the crystal structure of Fe film, we applied Fe K-edge EXAFS structural analysis to the film.

The results of the EXAFS experiment revealed that Fe atoms are not surrounded by only Fe atoms but also by O atoms, which suggests the existence of Fe oxides. Figure 12 shows the de-

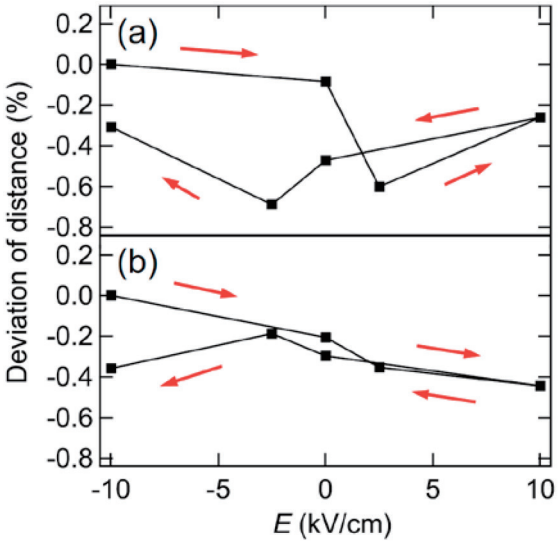

Fig. 12: Deviation of the in-plane bond distances for Fe–O (a) and Fe–Fe (b), as a function of the electric field, *E*. The electric field is changed from $E = -10$ kV/cm, as indicated by the arrows.

viation of the in-plane bond distances for Fe–O (a) and Fe–Fe (b), as a function of the electric field, *E*. Note that the electric field is changed from $E = -10$ kV/cm, as indicated by the arrows in the figure, and the deviation is estimated by setting the first point as a standard. The rate of change of the distance with respect to the electric field is larger for the Fe–O bond than for the Fe–Fe bond. This means that the local structure of the interfacial Fe oxide can be easily affected by the ferroelectric domain structure of the BTO substrate. Furthermore, the response to the electric field is very similar to that of M_0 and H_c as shown in Fig. 10. That is, the in-plane bond distance for Fe–O shows a hysteresis behavior, and shows a shorter distance at $\sim \pm 3$ kV/cm. These results indicate that the in-plane Fe–O distance is shorter when H_c is larger, in which the multi-domain structure in the BTO substrate is formed. On the other hand, the Fe–O distance is larger when H_c is smaller, in which BTO shows a single domain-like structure. In the former situation, the lateral connection of the Fe oxide over the grain boundary must be weak, and island-like localization is expected. We suppose that the localization of the interface Fe oxide leads to an enhancement of H_c of Fe.

Figure 13 shows PNR data for the 8-nm Fe film on the BTO substrate. A significant difference in the PNR curves is found especially at $q = 0.3-0.4$ and $0.5-0.6$ nm^{-1}, between 0 kV/cm and ± 1 kV/cm, which might reflect the difference in the domain structure of the BTO substrate. Further

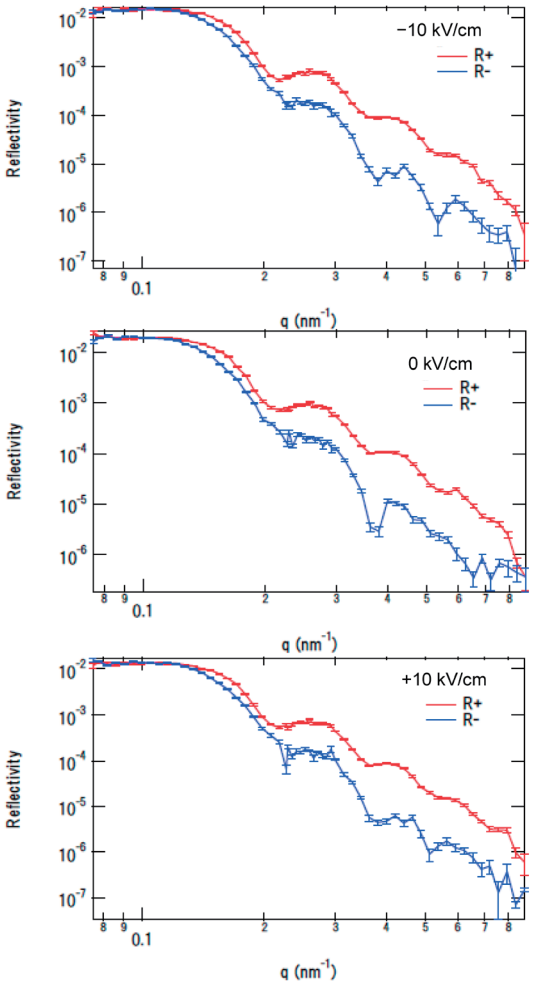

Fig. 13: PNR curves, R^+ and R^-, for 8-nm Fe film on BTO measured under different electric fields.

analysis is now under way in order to clarify the electric field dependence of the magnetic structure of Fe and Fe oxides at the interface with the BTO substrate.

We have also investigated the electric field dependence for many samples such as thinner (2 nm) Fe film grown on BTO, Fe/Fe_3O_4/BTO, Fe/NiO/BTO, and NiO/Ni/Cu(001), by complementarily using XMCD, EXAFS, and PNR techniques.

References

[1] K. Amemiya, Phys. Chem. Chem. Phys. **14** (2012) 10477.
[2] K. Amemiya et al., Appl. Phys. Lett. **84** (2004) 936.
[3] M. Takeda et al., Chin. J. Phys. **50** (2012) 161.
[4] M. Sakamaki and K. Amemiya, Appl. Phys. Express **4** (2011) 073002.
[5] M. Sakamaki and K. Amemiya, e-J. Surf. Sci. Nanotech. **10** (2012) 97.
[6] M. Sakamaki and K. Amemiya, Phys. Rev. B **87** (2013) 014428.

[7] M. Sakamaki and K. Amemiya, J. Phys.: Cond. Matter **26** (2014) 166002.
[8] K. Amemiya et al., Phys. Rev. B **89** (2014) 054404.
[9] K. Amemiya et al., JPS Conf. Proc., in press.
[10] M. Sakamaki et al., Phys. Rev. B **86** (2012) 024418.
[11] K. Amemiya et al., Eur. Phys. J. Web of Conf. **40** (2013) 08002.
[12] M. Sakamaki and K. Amemiya, e-J. Surf. Sci. Nanotech. **13** (2015) 139.
[13] K. Amemiya and M. Sakamaki, e-J. Surf. Sci. Nanotech. **13** (2015) 465.
[14] K. Amemiya et al., J. Phys.: Conf. Ser. **425** (2013) 152015.
[15] K. Tsuchiya et al., J. Phys.: Conf. Ser. **425** (2013) 132017.
[16] K. Amemiya et al., J. Phys.: Conf. Ser. **712** (2016) 012033.
[17] J. Wu et al., Phys. Rev. B **79** (2009) 212411.
[18] H. C. Choi et al., Phys. Rev. B **81** (2010) 224410.
[19] Y. Shiota et al., Nature Materials **11** (2012) 39.
[20] D. Khomskii, Physics **2** (2009) 20.
[21] S. Brivio et al., Appl. Phys. Lett. **98** (2011) 092505.